

Sliding charge density wave in manganites

Susan Cox,^{1*} J. Singleton,¹ R.D. McDonald,¹ A. Migliori,¹ P.B. Littlewood²

¹National High Magnetic Field Laboratory, Ms-E536, Los Alamos National Laboratory,
New Mexico, 87545, USA

²Cavendish Laboratory, University of Cambridge, Cambridge, CB3 0HE, UK

*e-mail:scox@lanl.gov

The so-called stripe phase of the manganites is an important example of the complex behaviour of metal oxides, and has long been interpreted as the localisation of charge at atomic sites^{1,2,3,4}. Here, we demonstrate via resistance measurements on $\text{La}_{0.50}\text{Ca}_{0.50}\text{MnO}_3$ that this state is in fact a prototypical charge density wave (CDW) which undergoes collective transport. Dramatic resistance hysteresis effects and broadband noise properties are observed, both of which are typical of sliding CDW systems. Moreover, the high levels of disorder typical of manganites result in behaviour similar to that of well-known disordered CDW materials. Our discovery that the manganite superstructure is a CDW shows that unusual transport and structural properties do not require exotic physics, but can emerge when a well-understood phase (the CDW) coexists with disorder.

The stripe phase in manganites of the form $\text{La}_{1-x}\text{Ca}_x\text{MnO}_3$ appears as the temperature is lowered through $T \simeq 240$ K, and the superstructure wavevector settles on a final value of $\mathbf{q} \simeq (1-x)\mathbf{a}^*$ (where \mathbf{a}^* is the reciprocal lattice vector) for $0.5 \leq x < 0.85$, at $T \simeq 120$ K². Based on the insulating nature of the manganites up to room temperature, and the observation of stripes of charge order in transmission electron microscopy (TEM) images, early studies concluded that the superstructure arose from localisation of charge at atomic sites^{3,4}. However, neutron and x-ray studies found the degree of charge localisation at Mn sites to be small, and subsequent theoretical work suggested that a CDW model may be more applicable⁵. This suggestion is supported by the observation that q/a^* is strongly temperature dependent^{2,6}, indicating that a model in which the superstructure periodicity is derived from the sample stoichiometry cannot be valid. In addition, heat capacity peaks at the transition to the stripe phase can be modelled as “dirty Peierls transitions”, expected in a disordered CDW system⁷. However, the possibility of the stripe phase exhibiting sliding behaviour, as seen in many other CDW systems⁸, could not be probed without the ability to make orientation-dependent resistivity measurements. Here we describe the first such measurements on the manganite stripe phase, which reveal dramatic

orientation-dependent resistivity and broadband noise effects which are characteristic of CDW sliding.

Orientation-dependent resistivity measurements require thin films, because untwinned single crystals of the insulating manganites cannot be grown⁹. The 80 nm thick $\text{La}_{0.5}\text{Ca}_{0.5}\text{MnO}_3$ thin film was grown on an NdGaO_3 substrate as described in¹⁰. The film was prepared for TEM by conventional grinding of the substrate to 50 μm and then milling a small window using a focused ion beam microscope to a thickness of around 200 nm. The sample was examined in a Philips CM30 microscope and was cooled to 90 K using a Gatan liquid nitrogen stage. The uniaxial stripe phase was identified via superlattice reflections in a selected area TEM diffraction pattern (illustrated below in Figure 2a); these reflections are detectable at 190 K, reaching a stable form at 90 K. (Note that previous resistivity measurements of thin film $\text{La}_{0.5}\text{Ca}_{0.5}\text{MnO}_3$ have failed to produce consistent results^{11,12,13}, because of the difficulty of producing high quality films and a failure to check for the superstructure using a microscopic technique.)

For the resistance measurements, gold wires were attached to the thin film sample using graphite paint. The differential resistivity of the sample studied here was measured by using a lock-in amplifier to detect the AC voltage produced in response to a 17 Hz AC current plus a DC bias; contacts were placed around the edges of the film to enable the current and bias to be applied along different directions, chiefly parallel and perpendicular to the superlattice direction. Both four-point and two-point configurations were employed for the resistivity experiments to eliminate possible contact resistance effects; the noise measurements reported below employed two contacts.

Analogies between $\text{La}_{0.5}\text{Ca}_{0.5}\text{MnO}_3$ and other CDW systems are clearly apparent in Figure 1, which shows the differential resistivity under zero DC bias versus temperature. The measurements appear similar to the resistivities of prototypical CDW systems doped with impurities^{14,15,16}, in that there is no clear feature at the expected CDW ordering temperature, with

insulating behaviour (i.e. decreasing resistivity with increasing temperature) persisting well above it. This has been interpreted as the “smearing” of the transition caused by the large impurity density^{14,15,16}. Analogous behaviour is also seen in cuprate ladder compounds exhibiting sliding density waves^{17,18} below $T \simeq 200$ K. As in the case of the cuprates, the resistivity of $\text{La}_{0.5}\text{Ca}_{0.5}\text{MnO}_3$ shows an activated temperature dependence with an activation energy which varies from $\simeq 1000 - 1400$ K (Figure 1b and c).

Figure 2 shows the differential resistivity as a function of DC bias applied parallel (along the lattice vector **a**) and perpendicular to (along the lattice vector **c**) the superlattice direction. At 157 K (Figure 2(f)), the differential resistivity drops in a similar fashion when the DC bias is applied in either direction. However, at temperatures $\lesssim 140$ K, the differential resistivity undergoes a sharp drop when the bias is applied in the **a** direction; the effect is very much less marked with the bias in the **c** direction (Figure 2(b)-(e)). In addition, there is a large hysteresis between the differential resistance recorded when the bias is first applied in the **a** direction after cooling from 300 K, and that measured on subsequent bias sweeps (in Figure 2 b-e the upper line in each direction shows the data from the first sweep after cooling and the lower line shows the data from subsequent sweeps); the area enclosed by the hysteresis loop increases rapidly as the temperature falls.

The hysteretic resistivity features shown in Figure 2 are typical of CDWs⁸. As the sample is cooled, the CDW settles into a minimum-free-energy pinned configuration, corresponding to maximum electrical resistivity⁸. On the application of electric field, the CDW initially undergoes local distortions that occur over longer and longer lengthscales as the field increases; eventually, the threshold field is reached and the CDW starts to slide. As the field is reduced again, the CDW freezes into a distorted state, characterized by a lower resistivity; the initial, minimum energy state cannot be regained without thermally cycling the sample⁸, explaining the hysteresis in our data.

Other mechanisms such as avalanche breakdown or sample heating cannot account for the data in Figure 2. Whilst these effects might produce a falling differential resistivity as the field increases, they would not produce a history-dependent result; on removing the field, the sample would return to its initial state. Moreover, whilst the DC resistivity for currents in the \mathbf{c} direction is 2 times higher than that for currents parallel to \mathbf{a} , the drop in resistivity as the field increases is five times larger in the latter direction (Figure 2); this anisotropy both fits naturally into the CDW picture and excludes heating and breakdown as possible mechanisms. The anisotropy in the observed effects also excludes ferromagnetic domains (sample inhomogeneity) as a possible mechanism; in this case the effects would be the same in the two orientations.

Having explained the hysteresis when the bias is along \mathbf{a} , we attribute the small amount of hysteresis seen when the bias is along \mathbf{c} (Figure 2) to imperfect contact geometry; i.e. misalignment results in a small amount of bias being applied in the perpendicular direction.

Another distinguishing feature of CDWs is that they exhibit a broadband noise spectrum with an amplitude proportional to $f^{-\alpha}$, where f is the frequency^{19,20,21,22,23}. Noise measurements were performed using a low-noise current source. The noise signal was amplified with a high input impedance, low noise preamplifier and was recorded via a digitizing oscilloscope. Lead capacitance, and the typical $10^6 \Omega$ sample resistance, limited noise measurements to below 10 kHz. Other techniques commonly used on CDW systems such as NbSe₃ were considered or attempted but typical properties of manganite films rendered them impossible; manganite film resistivities and geometries lead to RC time constants that are too high to perform experiments that measure effective pulse line or duration memory effects.

Figure 3 shows that significant broadband noise is observed in La_{0.5}Ca_{0.5}MnO₃ when the DC bias is applied in the superstructure direction. By contrast, the noise amplitude is much smaller with the bias in the non-superstructure direction. The exponent α in La_{0.5}Ca_{0.5}MnO₃ runs from 0.8 (156 K) to 2.0 (100 K), a similar range to values seen in the prototypical CDW

system NbSe_3 (0.8-1.8)⁸. However, the magnitude of the broadband noise in $\text{La}_{0.5}\text{Ca}_{0.5}\text{MnO}_3$ is much larger than that observed in clean CDW systems; for $\text{La}_{0.5}\text{Ca}_{0.5}\text{MnO}_3$ the effective noise temperature at 300 Hz is $\sim 10^{11}$ K for a sample temperature of 100 K, while in pure NbSe_3 the effective noise temperature is $\sim 10^6$ K. This is attributable to the large amount of disorder present in $\text{La}_{0.5}\text{Ca}_{0.5}\text{MnO}_3$ ⁷ (see above), so that there are many more pinning-depinning events compared to e.g. pure NbSe_3 . Although broadband noise has previously been observed in impurity-pinned CDWs²⁴, narrowband noise has not been observed in an impurity-doped or radiation-damaged sample, probably because the width of the narrowband noise peak is proportional to the magnitude of the broadband noise²². Therefore a high level of disorder or impurity pinning will lead to a large amount of broadband noise and unobservably small narrowband noise, as seen here in $\text{La}_{0.5}\text{Ca}_{0.5}\text{MnO}_3$.

As seen in other CDW systems²³, the amount of broadband noise decreases with increasing temperature (Figures 3a,c,e). For a bias above $E_T (\simeq 10^4 \text{V/m})$ in the superstructure direction this decrease is approximately linear with temperature (Figure 4c), as observed in the CDW system TaS_3 ²³. With the bias in the non-superstructure direction, the noise increases much more slowly; at 100 K it is more than an order of magnitude smaller than that with the bias along **a** (Figure 4c).

Figures 4a and b show the variation of the broadband noise amplitude with applied bias between the first bias sweep after cooling from 300 K and on a subsequent sweep. On first biasing, the noise amplitude shows a large peak at the same point as the large fall in differential resistance (Figure 4a). On subsequent bias sweeps, the noise increases more slowly with bias (Figure 4b). The large peak during the first bias sweep is caused by a high level of random telegraph signal (RTS) noise, which occurs in CDW systems as they switch from pinned to depinned states and back again^{25,26} close to the threshold field. The distinctive shape of the RTS noise is shown in Figure 4d, another factor adding weight to our identification of a CDW

in $\text{La}_{0.5}\text{Ca}_{0.5}\text{MnO}_3$.

In conclusion, we have demonstrated via resistivity and noise measurements that the superstructure in the stripe phase of manganites is a CDW which slides in the presence of an electric field. The manganite CDW is a fully gapped system with no screening electrons, which has previously only been observed in extremely clean organic materials²⁷. However, the manganite CDW exists with a high level of impurities, leading to dramatic hysteresis effects in the resistance. Our findings call for a reanalysis of the large region of the manganite phase diagram, $0.5 \leq x < 0.85$, which is occupied by the CDW. This is the first observation of sliding in a material which undergoes 3D charge ordering²⁸. In a wider context, this result is important because of the prevalence of stripe and checkerboard phases in oxide materials, including chelates, cobaltites, nickelates and cuprates; in particular, evidence is mounting that a glass of the stripe phase in cuprates is linked to high temperature superconductivity²⁹, making an understanding of the stripe phase a matter of urgency.

We thank N. Harrison, N.D. Mathur, P.A. Midgley, G. Kotliar and E. Rosten for helpful comments. S. Cox acknowledges support from the Seaborg institute. The sample was grown at Cambridge where research was funded by the UK EPSRC. This research was funded by the U. S. Department of Energy (DoE) under Grant ldrd-dr 20070013. Work at NHMFL is performed under the auspices of the NSF, the State of Florida, and the US DoE.

The authors declare no competing financial interests.

References

- [1] Chen, C. H., Mori, S. & Cheong, S.-W. Anomalous melting transition of the charge-ordered state in manganites. *Phys. Rev. Lett.*, **83**, 4792–4795, 1999.
- [2] Chen, C. H. & Cheong, S.-W. Commensurate to incommensurate charge ordering and its

- real-space images in $\text{La}_{0.5}\text{Ca}_{0.5}\text{MnO}_3$. *Phys. Rev. Lett.*, **76**, 4042–4045, 1996.
- [3] Chen, C. H., Cheong, S.-W. & Hwang, H.Y. Charge-ordered stripes in $\text{La}_{1-x}\text{Ca}_x\text{MnO}_3$ with $x > 0.5$. *J. Appl Phys*, **81**, 4326, 1997.
- [4] Mori, S., Chen, C. H. & Cheong, S.-W. Pairing of the charge-ordered stripes in $(\text{La,Ca})\text{MnO}_3$. *Nature*, **392**, 473–476, 1998.
- [5] Milward, G.C., Calderón, M.J., & Littlewood, P.B. Electronically soft phases in manganites. *Nature*, **433**, 607–610, 2005.
- [6] Loudon, J.C. *et al.* Weak charge-lattice coupling requires reinterpretation of stripes of charge order in $\text{La}_{1-x}\text{Ca}_x\text{MnO}_3$. *Phys. Rev. Lett.*, **94**, 097202/1–4, 2005.
- [7] Cox, S. *et al.* Evidence for the charge-density-wave nature of the stripe phase in manganites. *J. Phys.: Condens. Matter*, **19**, 192201/1–7, 2007.
- [8] G. Grüner. *Density waves in solids*. Addison-Wesley, 1994.
- [9] Majewski, P., Epple, L., Rozumek, M. & Schluckwerder, H. Phase diagram studies in the quasi binary systems $\text{LaMnO}_3\text{--SrMnO}_3$ and $\text{LaMnO}_3\text{--CaMnO}_3$. *J. Mater. Res.*, **15**, 1161–1166, 2000.
- [10] Cox, S. *et al.* Strain control of superlattice implies weak charge-lattice coupling in $\text{La}_{0.5}\text{Ca}_{0.5}\text{MnO}_3$. *Phys. Rev. B*, **73**, 132401/1–4, 2006.
- [11] Butorin, S.M., Sâthe, C., Saalem, F., Nordgren, J. & Zhu, X.M. Probing the Mn^{3+} sublattice in $\text{La}_{0.5}\text{Ca}_{0.5}\text{MnO}_3$ by resonant inelastic soft X-ray scattering at the Mn $L_{2,3}$ edge. *Surface Review and Letters*, **9**, 989–982, 2002.

- [12] Nyeanchi, E.B., Krylov, I.P., Zhu, X.-M. & Jacobs, N. Ferromagnetic ground state in $\text{La}_{0.5}\text{Ca}_{0.5}\text{MnO}_3$ thin films. *Euro. Phys. Lett.*, **48**, 228–232, 1999.
- [13] Xiong, Y.M. *et al.* Magnetotransport properties in $\text{La}_{1-x}\text{Ca}_x\text{MnO}_3$ ($x=0.33,0.5$) thin films deposited on different substrates. *J. Appl. Phys.*, **97**, 083909/1–11, 2005.
- [14] Ong, N.P. *et al.* Effect of impurities on the anomalous transport properties of NbSe_3 . *Phys. Rev. Lett.*, **42**, 811–814, 1979.
- [15] Brill, J.W. *et al.* Impurity effect on the frolich conductivity in NbSe_3 . *Phys. Rev. B*, **23**, 1517–1526, 1981.
- [16] Chaikin, P.M. *et al.* Thermopower of doped and damaged NbSe_3 . *Sol. Stat. Comm.*, **39**, 553–557, 1981.
- [17] Blumberg, G. *et al.* Sliding density wave in $\text{Sr}_{14}\text{Cu}_{24}\text{O}_{41}$ ladder compounds. *Science*, **297**, 584–587, 2002.
- [18] Maeda, A. *et al.* Sliding conduction by the quasi-one-dimensional charge-ordered state in $\text{Sr}_{14-x}\text{Ca}_x\text{Cu}_{24}\text{O}_{41}$. *Phys. Rev. B*, **67**, 115115/1–5, 2003.
- [19] Maeda, A., Naito, M. & Tanaka, S. Broad and narrow band noise of monoclinic TaS_3 . *Sol. Stat. Comm.*, **47**, 1001–1005, 1983.
- [20] Maeda, A., Naito, M. & Tanaka, S. Nonlinear conductivity and broad band noise of monoclinic TaS_3 . *J. Phys. Soc. Jpn.*, **54**, 1912–1922, 1985.
- [21] Richard, J., Monceau, P., Papoular, M. & Renard, M. $f^{-\alpha}$ noise in NbSe_3 . *J. Phys. C*, **15**, 7157–7164, 1982.

- [22] Maher, M.P. *et al.* Size effects, phase slip, and the origin of $f^{-\alpha}$ noise in NbSe₃. *Phys. Rev. B*, **43**, R9968–9971, 1991.
- [23] Zettl, A. & Grüner, G. Broad band noise associated with the current carrying charge density wave state in TaS₃. *Sol. Stat. Comm.*, **46**, 29–32, 1983.
- [24] Maeda, A., Uchinokura, K. & Tanaka, S. The effect of strong impurities on the low-frequency broad-band noise in NbSe₃. *Synthetic Metals*, **19**, 825–830, 1987.
- [25] Marley, A.C., Bloom, I. & Weissman, M.B. Temperature and electric-field dependences of characteristic noise patterns in mesoscopic ortho-TaS₃ charge density waves. *Phys. Rev. B*, **49**, 16156–16161, 1994.
- [26] Bloom, I., Marley, A.C. & Weissman, M.B. Discrete fluctuators and broad-band noise in the charge-density-wave in NbSe₃. *Phys. Rev. B*, **50**, 5081–5088, 1994.
- [27] McDonald, R.D. *et al.* Charge-density waves survive the pauli paramagnetic limit. *Phys. Rev. Lett.*, **93**, 076405/1–4, 2004.
- [28] Radaelli, P.G., Cox, D., Marezio, M., Cheong, S.-W, Schiffer, P.E. & Ramirez, A.P. Simultaneous structural, magnetic, and electronic transitions in La_{1-x}Ca_xMnO₃ with $x=0.25$ and 0.5. *Phys. Rev. Lett.*, **75**, 4488, 1995.
- [29] Kohsaka, Y. *et al.* An intrinsic bond-centered electronic glass with unidirectional domains in underdoped cuprates. *Science*, **315**, 1380–1385, 2007.

Figure 1: (a) Differential resistance of $\text{La}_{0.5}\text{Ca}_{0.5}\text{MnO}_3$ with the current in the **a** (red) and **c** (blue) directions versus temperature (zero DC bias). The resistivity is similar to that of the ladder compound $\text{Sr}_{14}\text{Cu}_{24}\text{O}_{41}$, shown in yellow¹⁷. (b) and (c) demonstrate that the resistivity is activated over all temperatures, being fitted to two exponentials.

Figure 2: (a) Linescan of TEM image in **a** (red) and **c** (blue) directions showing the superstructure reflections present in only the **a** direction. (b)-(f) Differential resistivity of $\text{La}_{0.5}\text{Ca}_{0.5}\text{MnO}_3$ versus DC bias with bias applied in the **a** (red) and **c** (blue) directions at various temperatures. In each case the upper curve is the differential resistivity obtained after cycling the temperature to 300 K, and the lower curve is the path followed by subsequent bias sweeps.

Figure 3: Frequency and current dependence of the broadband noise. 97 K data with the current parallel (a) and perpendicular (b) to q . 123 K data with the current parallel (c) and perpendicular (d) to q . 156 K data with the current parallel (e) and perpendicular (f) to q . The color scale is in units of V^2/Hz .

Figure 4: (a) Resistivity displayed as $R(E)/R(0)$ (red), and noise signal at 300 Hz (blue) for the first time current is passed parallel to the superstructure after cooling from 300 K. (b) Resistivity (red) and noise (blue) for the second time current is passed. (c) Noise signal at 300 Hz and 10 V as a function of temperature in the superstructure (red) and non-superstructure (blue) directions. The noise at 300 Hz was extracted by calculating the power spectral density of the noise and then taking the square root. Twenty points of the power spectral density were averaged. (d) Noise signal a short amount of time after the current has been changed; first (red) and second (blue) time the current is swept.

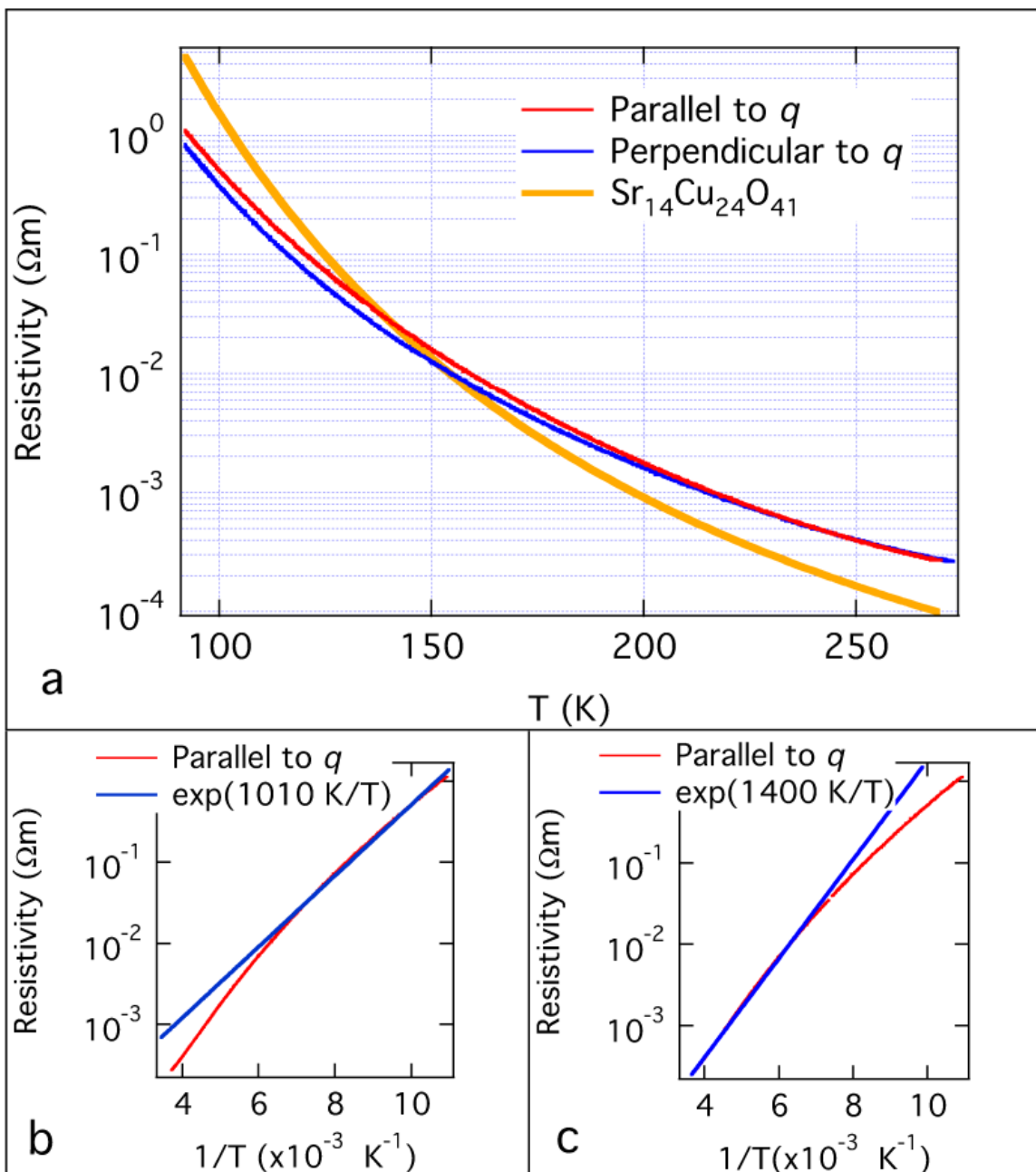


Figure 1:

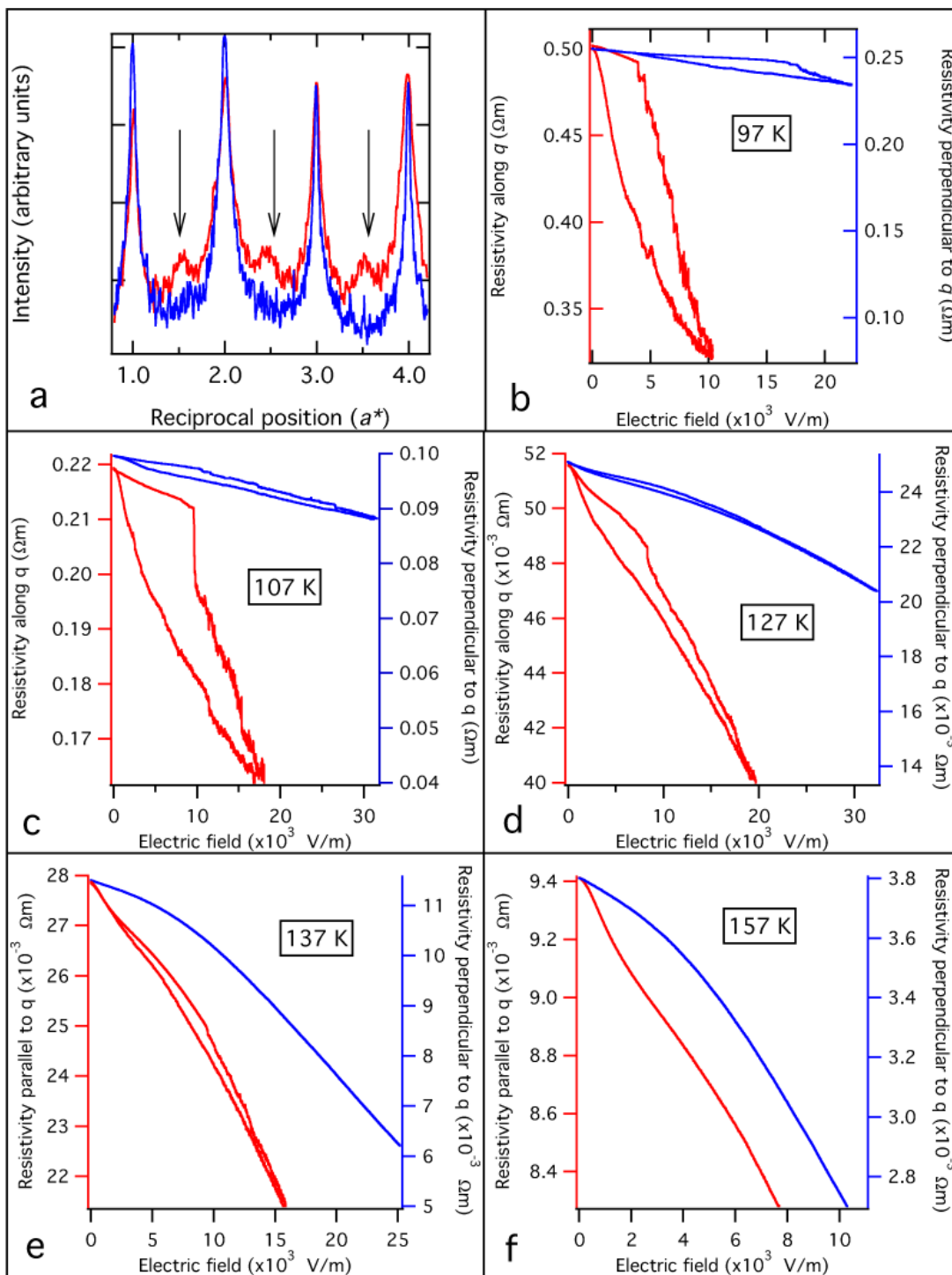


Figure 2:

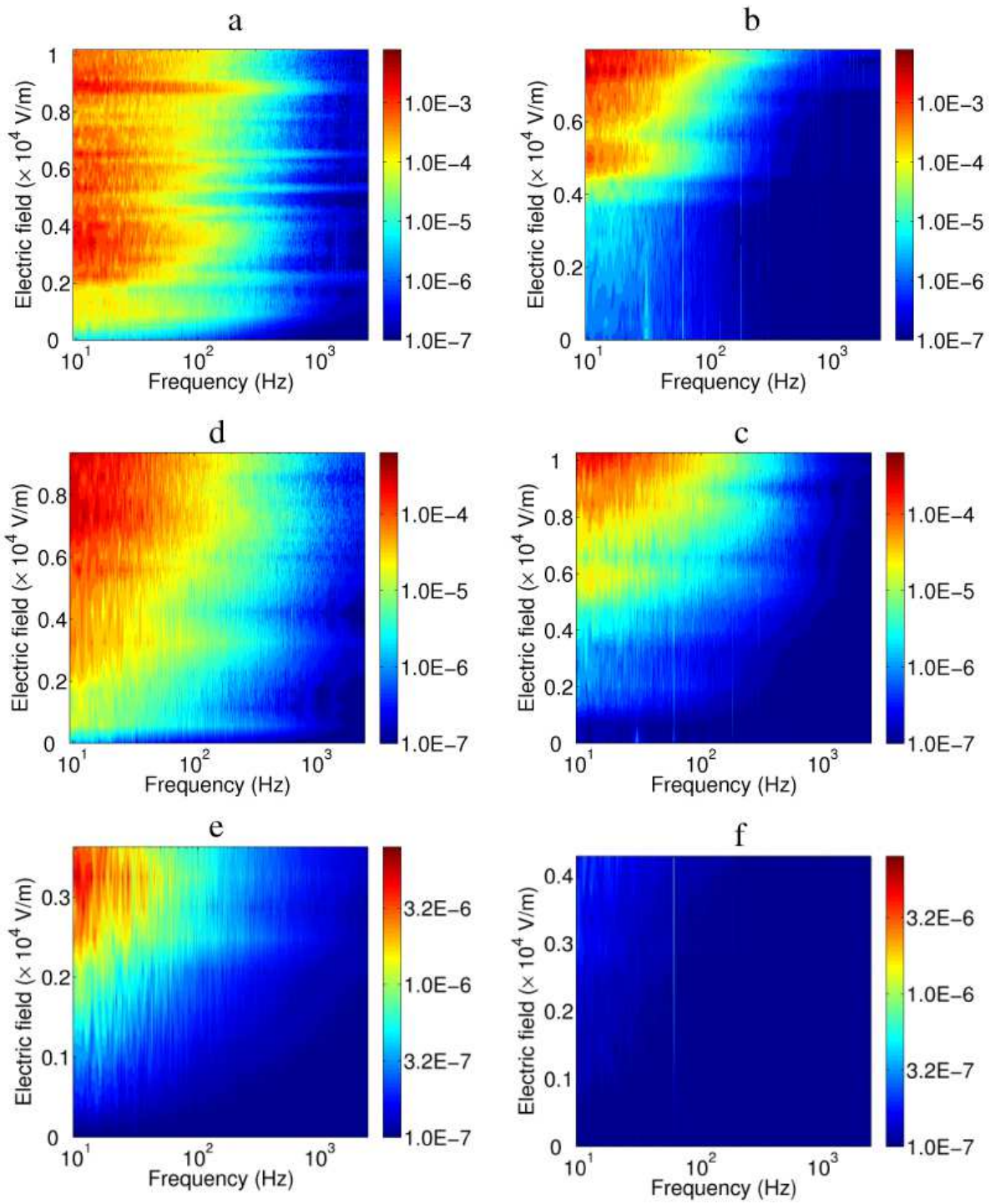


Figure 3:

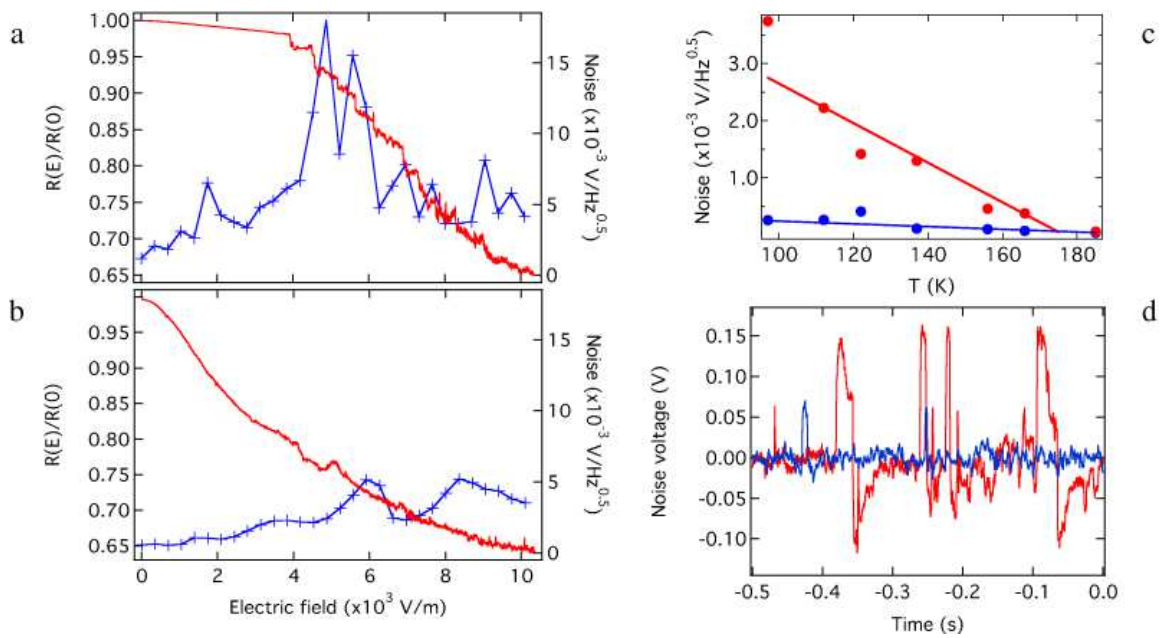


Figure 4: